CMS Physics Analysis Summary

Contact: cms-pag-conveners-higgs@cern.ch 2016/08/04

Search for non-resonant Higgs boson pair production in the $b\bar{b}\tau^+\tau^-$ final state using 2016 data

The CMS Collaboration

Abstract

A search for non-resonant Higgs boson pair production in the $b\bar{b}\tau^+\tau^-$ final state is presented. The search is performed using three $\tau\tau$ final states, $e\tau_h$, $\mu\tau_h$, and $\tau_h\tau_h$, where e and μ indicate a τ lepton decaying to lighter leptons and τ_h indicates a τ decay involving hadrons. The analysis uses proton-proton collision data collected in 2016 at 13 TeV and corresponding to an integrated luminosity of 12.9 fb^{-1}.

1 Introduction

The discovery of a Higgs boson (h) by the ATLAS and CMS Collaborations [1, 2] was a major step towards improving the understanding of the mechanism of electroweak symmetry breaking (EWSB). With the mass of the h boson now precisely determined [3], the structure of the Higgs scalar field potential and the Higgs boson self-couplings are precisely predicted in the Standard Model (SM). While measured properties are so far consistent with the expectation from the SM predictions [4], measuring the Higgs boson self-couplings through the trilinear Higgs boson coupling λ_{hhh} becomes of utmost importance to verify that the Brout-Englert-Higgs mechanism is truly responsible for EWSB. The self-interaction of the h boson via the triple coupling λ_{hhh} is accessible via pair production, which in pp collisions at the LHC mainly occurs in the SM via gluon fusion processes, involving either couplings to a loop of virtual fermions, or the λ_{hhh} coupling. The destructive interference between these main contributions makes the pair production of Higgs bosons particularly sensitive to physics beyond the SM (BSM) [5].

BSM physics can contribute to the pair production of Higgs bosons in various ways: via anomalous couplings to heavy SM quarks, new particles in the virtual loop at production, or via resonant enhancements. Note that this analysis attempts to search for an enhancement in the non-resonant pair production of Higgs bosons while the case of resonant production is documented elsewhere [6].

The BSM physics is modelled with an effective Lagrangian by adding dimension-6 operators to the SM Lagrangian [5], yielding three additional couplings c_2, c_{2g}, and c_g, denoting respectively the interactions of a top pair with a Higgs boson pair, of a gluon pair with a Higgs boson pair, and of a gluon pair with a single Higgs boson.

In this note, a search for non-resonant Higgs boson pair production is performed in the $\mathrm{bb}\tau\tau$ final state, one of the most promising, having a quite high branching ratio (7.3%) and a relatively small background contamination. The search is performed using the three most sensitive decay channels of the $\tau\tau$ system, $e\tau_{\mathrm{h}}$, $\mu\tau_{\mathrm{h}}$, and $\tau_{\mathrm{h}}\tau_{\mathrm{h}}$, where e and μ indicate a τ lepton decaying to lighter leptons and τ_{h} indicates a τ lepton decaying to hadrons.

Previous searches for the non-resonant production of a Higgs boson pair in the $\mathrm{bb}\tau\tau$ final state were performed by both the ATLAS and CMS collaborations using the LHC data collected at $\sqrt{s} = 8$ TeV [7, 8] and by the CMS collaboration using the 2.7 fb^{-1} of data collected during 2015 at $\sqrt{s} = 13$ TeV [9]. The best upper limit on non-resonant production cross section amounts to approximately 50 times the rate predicted by the SM [8].

2 The CMS Detector

A superconducting solenoid is the central feature of the CMS detector, providing an axial magnetic field of 3.8 T parallel to the beam direction. A silicon pixel and strip tracker, a crystal electromagnetic calorimeter (ECAL), and a brass/scintillator hadron calorimeter (HCAL) are located within the solenoid. A quartz-fiber Cherenkov calorimeter (HF) extends the forward coverage to $|\eta| < 5.0$, where $\eta = -\ln[\tan(\theta/2)]$. Muons are measured in gas-ionization detectors embedded in the steel flux return yoke outside the solenoid. The first level of the CMS trigger system, composed of custom hardware processors, is designed to select the most interesting events using information from the calorimeters and muon detectors. A high-level trigger processor farm decreases the event rate to about 1 kHz, before data storage. A more detailed description of the CMS detector, together with a definition of the coordinate system used and

the relevant kinematic variables, can be found in Ref. [10].

3 Datasets

The experimental data used for this search were recorded with the CMS detector in proton-proton collisions at the CERN LHC during Run-II and correspond to an integrated luminosity of 12.9 fb^{-1} at a centre-of-mass energy of $\sqrt{s} = 13\,\text{TeV}$.

Simulated signal and background samples are used to optimize the event selection and to evaluate the acceptance and systematic uncertainties.

The signal samples have been generated with MADGRAPH [11] for the SM and 12 BSM combinations of the effective Lagrangian coefficients introduced in Section 1. These 12 combinations are further detailed in Ref. [12]. Additional signal models corresponding to other combinations of the effective Lagrangian coefficients are obtained with an event weighting technique.

The numerical value of the hh SM cross section for the LHC centre-of-mass energies of 13 TeV at $m_{\text{h}} = 125\,\text{GeV}$ is $\sigma^{\text{SM}}_{gg\to\text{hh}}(13\text{TeV}) = 33.45\,\text{fb}\ ^{+4.3\%}_{-6.0\%}$(scale unc.) $\pm 2.1\%$(PDF unc.)$\pm 2.3\%$(α_S unc.) [13]. It is calculated at NNLL matched to NNLO cross sections [14–16] including top quark mass effects to NLO [17], and using the PDF4LHC recommendations for LHC Run-II [18] with the renormalisation and factorisation scales set to $m_{hh}/2$. The cross sections for anomalous couplings are calculated using the results presented in Ref. [19].

The Z+jets, W+jets, and di-boson background samples have been generated with MADGRAPH and $\text{t}\bar{\text{t}}$ and single top with POWHEG [20, 21]. For the Z+jets and W+jets backgrounds, separate samples generated for different numbers and flavors of outgoing partons in the hard interaction process are combined to enhance the background event statistics in regions of high signal purity.

The $\text{t}\bar{\text{t}}$, Z+jets, and W+jets samples are normalized to their respective NNLO cross sections [22]. A kinematic weighting is applied to the $\text{t}\bar{\text{t}}$ simulation to better match the top quark p_{T} distribution observed in data. The single-top and di-boson samples are normalized to their respective NLO cross sections.

Hadronic shower and hadronization processes are modelled using PYTHIA (v.8.2) [23].

During the 2016 LHC run there were an average of 18 pp interactions per bunch crossing. The simulation includes the effects of the overlapping pp interactions (pileup). Simulated events are weighted to match the simulated pileup distribution to the one measured in data.

4 Event reconstruction

The event reconstruction is based on the particle-flow (PF) algorithm [24, 25], which aims to exploit the information from all subdetectors to identify individual particles as PF candidates: charged and neutral hadrons, muons, electrons, and photons. Complex objects, such as τ leptons that decay into hadrons and a neutrino, jets, and the imbalance in the transverse momentum in the event $E_{\text{T}}^{\text{miss}}$, are reconstructed from PF candidates.

The deterministic annealing algorithm [26, 27] is used to reconstruct the collision vertices. The vertex with the maximum sum of squared transverse momenta (p_{T}^2) of all associated tracks is considered as the primary vertex. Muons, electrons, and τ leptons decaying into hadrons and a neutrino (τ_{h}) are required to originate from the primary collision vertex.

The electron reconstruction combines ECAL and tracker information. Electron candidates are reconstructed from clusters of energy deposits in the ECAL, which are then matched to hits in the silicon tracker. The standard CMS electron reconstruction algorithm is used for this analysis [28]. Electrons are identified using a multivariate approach (MVA) and the method has been updated and improved for the Run-II analyses. The discriminator is based on a Boosted Decision Tree (BDT) [29], that combines observables sensitive to the amount of bremsstrahlung along the electron trajectory, the geometrical and momentum matching between the electron trajectory and associated clusters, shower-shape observables, and the number of missing hits along the electron track.

The muon reconstruction starts by matching tracks in the silicon tracker with tracks in the outer muon spectrometer [30]. A global muon track is fitted to the hits from both tracks.

Electron and muon isolations I_l^{rel}, measured relative to their transverse momentum, are defined by the sums over charged particles, neutral particles, and photons reconstructed with the PF algorithm in a cone $\Delta R = \sqrt{(\Delta\eta)^2 + (\Delta\phi)^2} < 0.4$ around the lepton direction at the interaction vertex, where $\Delta\eta$ and $\Delta\phi$ quantify the angular distance of the PF candidate from the lepton in the η and ϕ directions. The isolation is corrected to take into account effects from pileup.

Jets are reconstructed from PF candidates using the anti-k_{T} [31] algorithm with a distance parameter of 0.4, in the FASTJET package [32]. Jets from the hadronisation of b-quarks (b jets) are identified with the combined secondary vertex (CSVv2) b tagging algorithm [33], based on neural network algorithms tuned for Run-II analyses, and exploits information such as the impact parameters of charged-particle tracks and the properties of reconstructed decay vertices.

Decays of τ leptons involving hadrons are reconstructed by the Hadrons plus Strips (HPS) identification algorithm [34, 35]. This algorithm is seeded from a particle flow jet, and searches for candidates produced by the main hadronic decay modes of the τ lepton: either directly to one charged hadron, or via intermediate $\rho(770)$ and $\mathrm{a}_1(1280)$ mesons to one charged hadron plus one or two neutral pions, or three charged hadrons with up to one neutral pion. The charged hadrons are usually long-lived pions, while the neutral pions decay rapidly into two photons. The HPS algorithm takes into account the possible conversion of photons into $\mathrm{e}^+\mathrm{e}^-$ pairs in material in front of the ECAL, and their corresponding bremsstrahlung in the magnetic field with consequent broadening of the distribution of the shower. Strips are formed with dynamic size from energy depositions in the ECAL arising from electrons and photons. The τ decay modes are reconstructed by combining the charged hadrons with ECAL strips. Neutrinos produced in τ decays are not reconstructed but contribute to the missing transverse energy, $E_{\mathrm{T}}^{\mathrm{miss}}$, that is reconstructed using the particle-flow algorithm [24]. The τ isolation (I_τ) is computed by summing the transverse momenta of charged particles and photons reconstructed with the PF algorithm, within an isolation cone of size $\Delta R = 0.5$, centered around the τ direction. Charged hadrons and photons that are associated to the τ candidate decay are excluded from the p_T-sum. The isolation is corrected to take into account effects from pileup.

5 Event selection

Three channels are analyzed, distinguished by the decay mode of the two τ leptons originating from one Higgs boson. These channels are denoted as $\mathrm{bb}e\tau_{\mathrm{h}}$, $\mathrm{bb}\mu\tau_{\mathrm{h}}$, and $\mathrm{bb}\tau_{\mathrm{h}}\tau_{\mathrm{h}}$. The events used in this search are recorded using a set of triggers that relies on the information from the identification of electrons, muons and τ leptons.

The data analyzed in the $\mu\tau_{\mathrm{h}}$ ($e\tau_{\mathrm{h}}$) channel were collected with a trigger that required the

presence of a muon (electron) in the event. In the offline selection, the events selected with these triggers are required to contain a reconstructed muon (electron) of $p_T > 23(27)$ GeV and $|\eta| < 2.1$ and a reconstructed τ_h of $p_T > 20$ GeV and $|\eta| < 2.3$. The muon and electron candidates are required to pass the relative isolation requirement $I_l^{rel} < 0.1$, while for τ_h isolation is required with $I_\tau < 3$ GeV. Additional discriminators are applied to the τ_h candidate to reject electrons and muons wrongly reconstructed as τ decays involving hadrons.

The trigger used for the $bb\tau_h\tau_h$ channel requires the presence of two τ_h candidates in the event. In the offline selection, the events selected with this trigger are required to contain two reconstructed τ_h of $p_T > 45$ GeV and $|\eta| < 2.1$. Both τ_h candidates are required to pass the isolation requirement of $I_\tau < 2$ GeV. The discriminators against electrons and muons are applied to both τ_h candidates.

For all three channels, the two selected leptons are required to have opposite charge. Events containing additional isolated electrons or muons are rejected to reduce the Drell-Yan background contribution.

All events selected with the previous criteria are required to have two additional jets with $p_T > 30$ GeV and $|\eta| < 2.4$. Jets are required to pass a working point of the b-tag discriminator defined to have a mistag rate of 10^{-1}.

The invariant mass of the $\tau\tau$ system is reconstructed using a likelihood technique as documented in Ref. [36]. Two requirements on the invariant mass of the $\tau\tau$ and bb pair are applied to reject events that are not compatible with the hypothesis of two Higgs bosons of 125 GeV mass. Both the $\tau\tau$ reconstructed invariant mass and the bb invariant mass are required to be in the interval $80\,\text{GeV} < m_{\tau\tau}(m_{bb}) < 160\,\text{GeV}$.

In addition to the previous requirements, a multivariate discriminator is applied in the $bb\mu\tau_h$ and $bbe\tau_h$ channels. It consists in a BDT trained to discriminate signal-like events from $t\bar{t}$ events, the latter being the most important source of background in these two final states. The discriminator is not used in the $bb\tau_h\tau_h$ channel where the major contribution comes from multijet background that has different kinematic properties. Only angular variables not affected by NLO effects have been chosen as input to the BDT ensuring a good signal to background discrimination and at the same time showing moderate dependency on the value of λ_{hhh}. The five variables used are: $\Delta\varphi(h_{bb}, h_{\tau\tau})$, $\Delta\varphi(h_{\tau\tau}, E_T^{miss})$, $\Delta\varphi(h_{bb}, E_T^{miss})$, $\Delta R(b,b)$, and $\Delta R(l, \tau_h)$ with $l = e, \mu$, where h_{bb} ($h_{\tau\tau}$) denotes the Higgs boson four-momentum reconstructed from the bb ($\tau\tau$) candidates pair, $\Delta\varphi$ denotes the angular separation in the trasverse plane, and ΔR is the separation between the two objects (e, μ, τ_h, and b) computed over the whole detector as $\Delta R = \sqrt{\Delta\eta^2 + \Delta\varphi^2}$.

The training of the BDT is performed using the standard model sample as signal and the $t\bar{t}$ MC sample for the background. Given the similarities in the kinematics of the $bb\mu\tau_h$ and $bbe\tau_h$ channels, the BDT is trained using the two decay channels together in order to increase the sample statistics.

The distribution of the BDT output is shown in Fig. 1a for the $bb\mu\tau_h$ channel and in Fig. 1b for the $bbe\tau_h$ channel before the application of the selection on the invariant masses. The expected SM signal contribution is shown for a value of the SM cross section multiplied by a factor 10^4 and the separation of signal and background distributions is clearly visible. The selection on the BDT output has been chosen such that a signal efficiency of 80% is achieved, corresponding to a background rejection of about 85%. This working points corresponds to a BDT score of -0.134.

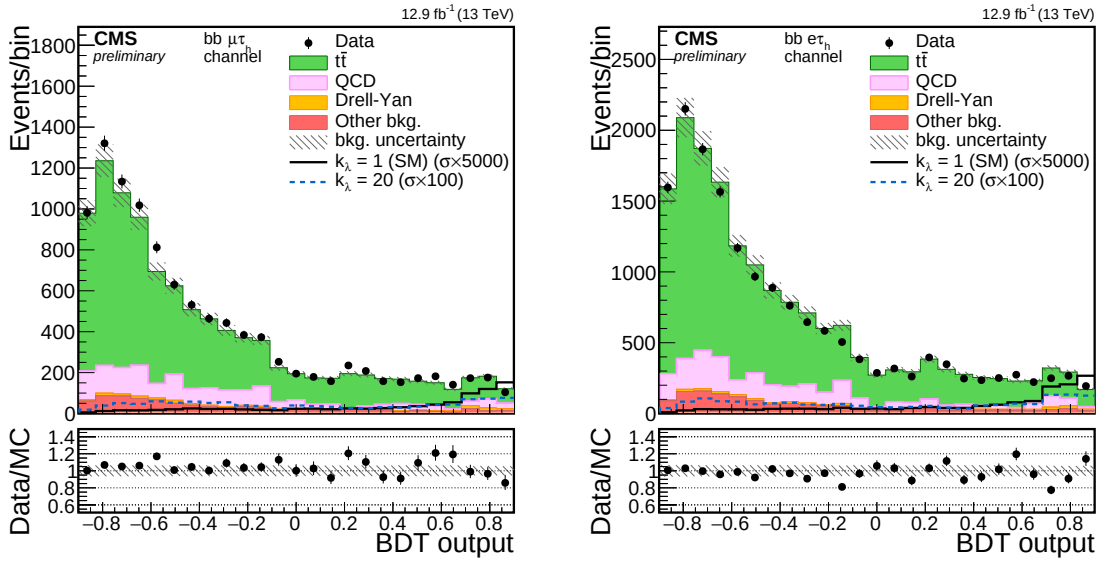

(a) bb$\mu\tau_h$ (b) bb$e\tau_h$

Figure 1: Output of the BDT discriminator in the bb$\mu\tau_h$ channel (a) and bb$e\tau_h$ channel (b). Points with error bars represent the data and shaded histograms represent the backgrounds. The black unshaded histogram is the signal expectation for the SM ($k_\lambda = \lambda_{hhh}/\lambda_{hhh}^{SM} = 1$) and the blue dashed unshaded histogram is the signal expectation for $k_\lambda = 20$. The SM production cross section is scaled by a factor 5000 and the $k_\lambda = 20$ production cross section is scaled by a factor 100. Signal and background histograms are not stacked. The lower panel shows the ratio of the observed data to the MC prediction.

6 Background estimation

The multijet background is determined from data using a jet-enriched region. The yield is obtained from the same-sign (SS) region defined in the same way as the signal region except that the two τ lepton candidates are required to have the same electric charge. The events in this region are scaled by the ratio of opposite-sign (OS) to SS event yields obtained in a multijet enriched region with relaxed lepton isolation. The contributions of other backgrounds are subtracted in the OS and SS regions based on MC predictions. The shape of the multijet background is estimated using an observed sample of SS $\tau\tau$ events with relaxed τ isolation.

The contribution of the $\mathrm{t\bar{t}}$ background is modelled in shape using the MC simulation. CMS measurements of the differential $\mathrm{t\bar{t}}$ production cross section at 13 TeV [37] indicate that the kinematics of the process is overall well modelled; to account for small discrepancies between data and MC shape, the $\mathrm{t\bar{t}}$ shape is corrected as described in Section 3. The contribution is normalized to the theoretical prediction computed at NNLO precision [22].

The contribution of the Z+jets background is modelled in shape using the MC simulation, and is normalized to the theoretical prediction computed at NNLO precision. To account for possible imprecisions in the modeling of the jets emission in the MC simulations, the expected event contribution is corrected by multiplicative correction factors derived in three separate control regions dominated by the Z+jets background and defined by the presence of two muons of invariant mass $80\,\mathrm{GeV} < m_{\mu\mu} < 100\,\mathrm{GeV}$ and two jets of invariant mass $80\,\mathrm{GeV} < m_{jj} < 160\,\mathrm{GeV}$. The three regions are defined by the number of b-tagged jets in the final state (0, 1 or $\geq$ 2). The Z+jets MC sample is divided in three components according to the number of generator level jets with B hadrons (0, 1 or $\geq$ 2), and the event yields from the three components are

simultaneously fitted to the data in the three control regions to derive the correction factors.

The background contributions arising from W+jets, single top, and di-boson production are subdominant when compared to the total background yield and are modelled relying solely on the MC simulation.

7 Systematic uncertainties

Several sources of systematic uncertainties that are due to the imperfect knowledge of the detector response or discrepancies between MC simulation and data are considered in the analysis. Systematic uncertainties are separately treated as "normalization" uncertainties or "shape" uncertainties; the first type affects the number of expected events from a background process, while the second type affects their templated shapes.

7.1 Normalization uncertainties

- An uncertainty of 6.2% is considered to cover the uncertainty on the luminosity measurement and it is considered fully correlated among all the final states. This value is obtained from dedicated Van-der-Meer scans and stability of detector response during the data taking. The uncertainty is applied to the signal and to $\bar{\text{t}}\text{t}$, W+jets, single top, and di-boson backgrounds. It is not applied on the multijet and Z+jets backgrounds because they are estimated or corrected from data.
- The uncertainties on electron and muon trigger, identification and isolation efficiencies are determined from the uncertainties on the Monte Carlo-to-data correction factors. The uncertainties are considered as uncorrelated and a value of 3% for electrons and a value of 2% for muons are obtained.
- The uncertainty on the τ_h identification efficiency has been measured during Run-II using $Z/\gamma^* \to \tau\tau \to \mu\tau_h$ events and amounts to 6% [38].
- An uncertainty on each τ_h candidate coming from τ energy scale correction is introduced by varying each τ momentum by 3% up and down. This results in a normalization uncertainty of 3-10% depending on the process, and it is fully correlated with a corresponding shape uncertainty on the visible hh mass distribution.
- Uncertainties on Monte Carlo-to-data b-tagging efficiencies correction factors as function of jet p_T and η are evaluated by observing the changes in the normalization when varying the correction factors around the nominal value inside the error boundaries, obtaining an average value of 2-6% for the samples with true b-jets in the final states.
- Uncertainties arising from the imperfect knowledge of the jet measured energy are estimated by evaluating the changes in the yield after the bb invariant mass requirement when both b jet momenta are scaled inside the errors. The estimation leads to an uncertainty of about 2% (4%) for signal (background).
- The theoretical uncertainties on the signal cross section are due to the scale uncertainties of $+4.3/-6\%$ and to the PDF+α_S uncertainties of 3.1%.
- The uncertainties on background normalization due to the imperfect knowledge of their cross sections are added as uncorrelated from other sources of systematics. This uncertainty is applied for $\bar{\text{t}}\text{t}$, W+jets, single top, and di-boson backgrounds using the error from the theoretical computation.
- The uncertainties on the three correction factors for the Z+jets background are prop-

Table 1: Systematic uncertainties affecting the normalization of the different processes.

Systematic	value	processes
luminosity	6.2%	all but multijet, Z+jets
Jet energy scale	2-4%	all
MC cross-section	1-10%	backgrounds, not Z+jets, multijet
b-tag efficiency	2-6%	all
lepton efficiency	2-6%	all
Z+jets SF uncertainty	1-10%	Z+jets
τ energy scale	3-10%	all
scale unc.	$+4.3/-6\%$	theory
PDF variation	3.1%	theory

agated from the fit in the control region to the signal region, taking into account the correlation between the three factors in the statistical treatment.

- The uncertainty on the multijet background yield is estimated by propagating the statistical uncertainties on the number of events used for its determination in the region with the sign requirement inverted, as described in Section 6.

7.2 Shape uncertainties

- Differences in the differential p_T distribution between data and Monte Carlo simulation for the $t\bar{t}$ process are corrected with an event weighting method as described in Section 3. The error arising from this procedure is determined by computing two alternative shapes in the absence of reweighting and applying two times the event weights.
- The multijet background shape uncertainty is assessed from the error in the correction applied on the shape determined in the region with relaxed isolation.
- Uncertainties due to the limited number of simulated events or due to the limited number of events in the multijet control region are taken into account. These uncertainties are uncorrelated across bins in the individual templated shapes.
- Uncertainty on the visible mass distribution coming from the upward and downward shift of the τ energy scale.

8 Results

The numbers of expected and observed events in the $bb\mu\tau_h$, $bbe\tau_h$, and $bb\tau_h\tau_h$ final states are given in Table 2.

Figure 2 shows the distributions of the reconstructed four-body mass, the final discriminating variable to extract the results, after applying mass selections on $m_{\tau\tau}$ and m_{bb} in all the final states and in addition the cut on the kinematical BDT score in the $bb\mu\tau_h$ and $bbe\tau_h$ final states.

In the absence of evidence for a signal, we proceed by setting 95% CL upper limits on cross section times branching ratio for the non-resonant Higgs boson pair production, as a function of the ratio of the anomalous trilinear coupling to the SM trilinear coupling ($k_\lambda = \lambda_{hhh}/\lambda_{hhh}^{SM}$) as shown in Fig. 3.

For non-resonant Higgs boson pair production at $k_\lambda = 1$ the observed (expected) limit on $\sigma(pp \to hh \to bb\tau\tau)$ amounts to 508 (420) fb. This value corresponds to approximately 200 (170) times the SM prediction.

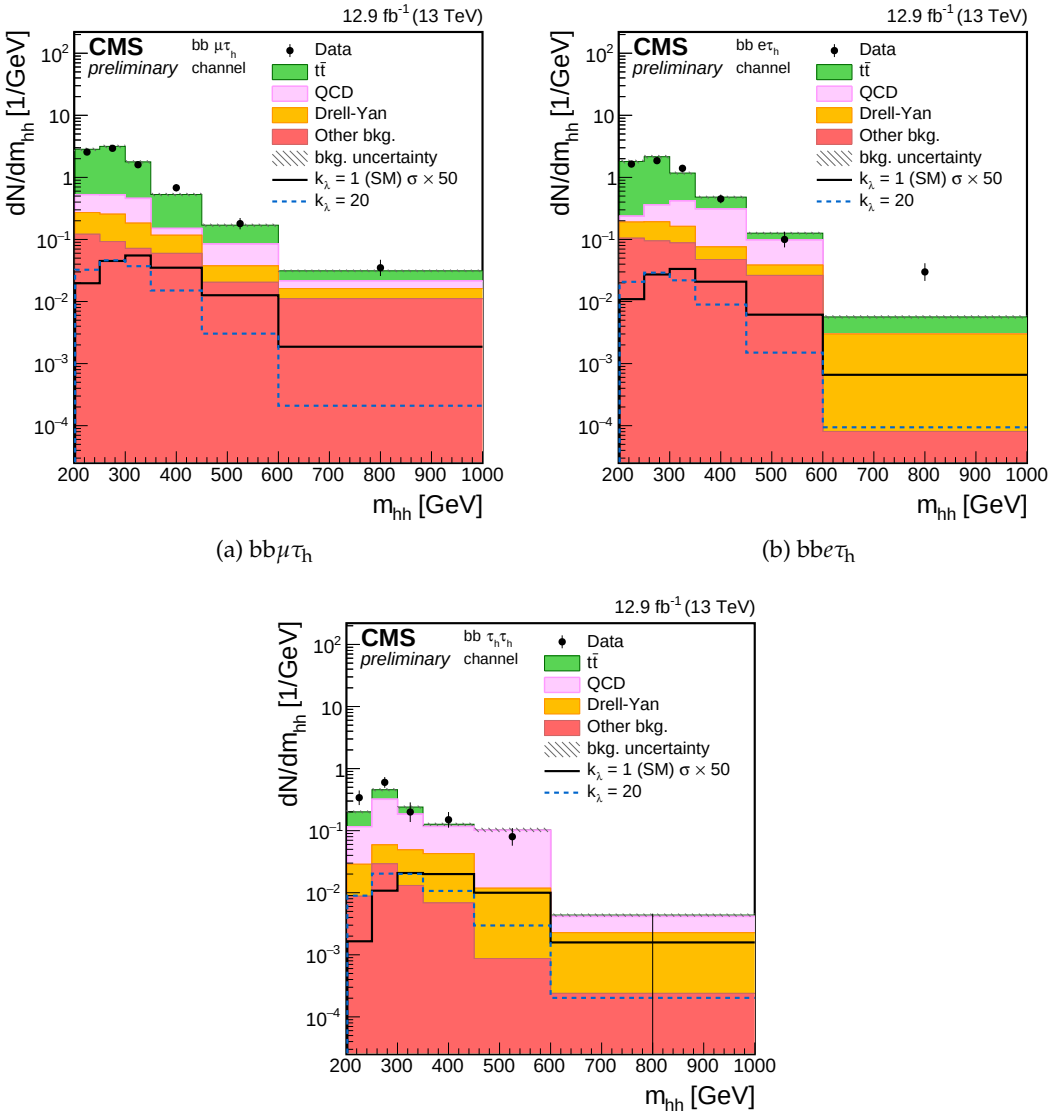

(a) bb$\mu\tau_h$ (b) bb$e\tau_h$

(c) bb$\tau_h\tau_h$

Figure 2: Distributions of the reconstructed visible four-body mass (m_{hh}) after applying the event selection. The plots are shown for (a) bb$\mu\tau_h$, (b) bb$e\tau_h$, and (c) bb$\tau_h\tau_h$ channels. Points with error bars represent the data, shaded histograms represent the backgrounds, the black unshaded histogram is the signal expectation for the SM ($\lambda_{hhh}/\lambda^{SM}_{hhh} = 1$), and the blue dotted unshaded histogram is the signal expectation for $\lambda_{hhh}/\lambda^{SM}_{hhh} = 20$. The SM production cross section is scaled by a factor 50. Event yields in each bin are divided by the bin width. Expected background contributions are shown for the values of nuisance parameters (systematic uncertainties) obtained after fitting the background hypothesis to the data. Signal and background histograms are not stacked.

Table 2: Observed and expected event yields in different event final states. Quoted uncertainties represent the combination of statistical plus systematic uncertainties.

Process	$bb\mu\tau_h$	$bbe\tau_h$	$bb\tau_h\tau_h$
$t\bar{t}$	368.1 ± 37.2	228.5 ± 23.4	15.3 ± 1.7
multijet	52.2 ± 6.5	55.7 ± 4.6	45.7 ± 4.1
Z+jets	31.5 ± 3.0	18.7 ± 1.9	10.3 ± 1.1
W+jets	13.0 ± 1.0	11.0 ± 0.9	1.4 ± 0.1
single top	11.6 ± 1.0	10.7 ± 1.0	1.5 ± 0.2
di-boson	3.1 ± 0.4	1.4 ± 0.2	0.7 ± 0.1
Total expected background	480.0 ± 37.9	326.0 ± 24.4	74.8 ± 4.6
$k_\lambda = 1$	0.24	0.13	0.12
$k_\lambda = 20$	7.8	4.8	4.1
DATA	464	317	84

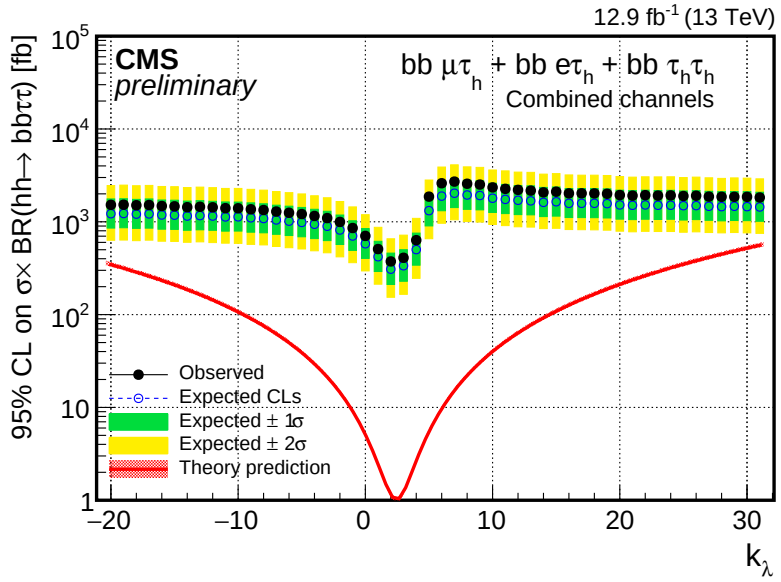

Figure 3: Observed and expected 95% CL upper limits on cross section times branching ratio as a function of the ratio of the anomalous trilinear coupling to the SM trilinear coupling ($k_\lambda = \lambda_{hhh}/\lambda_{hhh}^{SM}$) combining all the final states. The red band shows the theoretical cross section expectation and its systematic uncertainty

9 Summary

The search for non-resonant Higgs boson pair production in the $\mathrm{bb}\tau\tau$ final state with a collected luminosity of 12.9 fb^{-1} at $\sqrt{s} = 13$ TeV is presented. The search is performed using the three most sensitive decay channels of the τ leptons, $e\tau_\mathrm{h}$, $\mu\tau_\mathrm{h}$, and $\tau_\mathrm{h}\tau_\mathrm{h}$, where τ_h indicates a tau decay involving hadrons. For non-resonant Higgs boson pair production at $k_\lambda = 1$ the observed (expected) 95% CL upper limit on $\sigma(\mathrm{pp} \to \mathrm{hh} \to \mathrm{bb}\tau\tau)$ amounts to 508 (420) fb. This value corresponds to approximately 200 (170) times the SM prediction.

References

[1] ATLAS Collaboration, "Observation of a new particle in the search for the Standard Model Higgs boson with the ATLAS detector at the LHC", *Physics Letters B* **716** (2012), no. 1, 1 – 29, doi:10.1016/j.physletb.2012.08.020.

[2] CMS Collaboration, "Observation of a new boson at a mass of 125 GeV with the CMS experiment at the LHC", *Physics Letters B* **716** (2012), no. 1, 30 – 61, doi:10.1016/j.physletb.2012.08.021.

[3] ATLAS, CMS Collaboration, "Combined Measurement of the Higgs Boson Mass in pp Collisions at $\sqrt{s} = 7$ and 8 TeV with the ATLAS and CMS Experiments", *Phys. Rev. Lett.* **114** (2015) 191803, doi:10.1103/PhysRevLett.114.191803, arXiv:1503.07589.

[4] CMS Collaboration, "Measurements of the Higgs boson production and decay rates and constraints on its couplings from a combined ATLAS and CMS analysis of the LHC pp collision data at $\sqrt{s}$ = 7 and 8 TeV", CMS Physics Analysis Summary CMS-PAS-HIG-15-002, CERN, Geneva, 2015.

[5] S. Dawson, A. Ismail, and I. Low, "What's in the loop? The anatomy of double Higgs production", *Phys. Rev.* **D91** (2015), no. 11, 115008, doi:10.1103/PhysRevD.91.115008, arXiv:1504.05596.

[6] CMS Collaboration, "Search for resonant Higgs boson pair production in the $\mathrm{b\bar{b}}\tau^+\tau^-$ final state", CMS Physics Analysis Summary CMS-PAS-HIG-16-029, 2016.

[7] ATLAS Collaboration, "Searches for Higgs boson pair production in the $hh \to bb\tau\tau, \gamma\gamma WW^*, \gamma\gamma bb, bbbb$ channels with the ATLAS detector", *Phys. Rev.* **D92** (2015) 092004, doi:10.1103/PhysRevD.92.092004, arXiv:1509.04670.

[8] CMS Collaboration, "Model independent search for Higgs boson pair production in the $\mathrm{b\bar{b}}\tau^+\tau^-$ final state", CMS Physics Analysis Summary CMS-PAS-HIG-15-013, 2016.

[9] CMS Collaboration Collaboration, "Search for non-resonant Higgs boson pair production in the $\mathrm{b\bar{b}}\tau^+\tau^-$ final state", CMS Physics Analysis Summary CMS-PAS-HIG-16-012, CERN, Geneva, 2016.

[10] CMS Collaboration, "The CMS experiment at the CERN LHC", *JINST* **3** (2008) S08004, doi:10.1088/1748-0221/3/08/S08004.

[11] J. Alwall et al., "The automated computation of tree-level and next-to-leading order differential cross sections, and their matching to parton shower simulations", *JHEP* **07** (2014) 079, doi:10.1007/JHEP07(2014)079, arXiv:1405.0301.

[12] A. Carvalho Antunes De Oliveira et al., "Analytical parametrization and shape classification of anomalous HH production in EFT approach", LHCHXSWG report LHCHXSWG-2016-001, CERN, Geneva, Jul, 2016.

[13] B. Mellado Garcia, P. Musella, M. Grazzini, and R. Harlander, "CERN Report 4: Part I Standard Model Predictions", CERN Report LHCHXSWG-DRAFT-INT-2016-008, May, 2016.

[14] S. Dawson, S. Dittmaier, and M. Spira, "Neutral Higgs boson pair production at hadron colliders: QCD corrections", *Phys. Rev.* **D58** (1998) 115012, doi:10.1103/PhysRevD.58.115012, arXiv:hep-ph/9805244.

[15] D. de Florian and J. Mazzitelli, "Higgs Boson Pair Production at Next-to-Next-to-Leading Order in QCD", *Phys. Rev. Lett.* **111** (2013) 201801, doi:10.1103/PhysRevLett.111.201801, arXiv:1309.6594.

[16] D. de Florian and J. Mazzitelli, "Higgs pair production at next-to-next-to-leading logarithmic accuracy at the LHC", *JHEP* **09** (2015) 053, doi:10.1007/JHEP09(2015)053, arXiv:1505.07122.

[17] S. Borowka et al., "Higgs boson pair production in gluon fusion at NLO with full top-quark mass dependence", arXiv:1604.06447.

[18] J. Butterworth et al., "PDF4LHC recommendations for LHC Run II", arXiv:1510.03865.

[19] A. Carvalho et al., "Higgs Pair Production: Choosing Benchmarks With Cluster Analysis", *JHEP* **04** (2016) 126, doi:10.1007/JHEP04(2016)126, arXiv:1507.02245.

[20] S. Alioli, P. Nason, C. Oleari, and E. Re, "NLO single-top production matched with shower in POWHEG: s- and t-channel contributions", *JHEP* **09** (2009) 111, doi:10.1007/JHEP02(2010)011, 10.1088/1126-6708/2009/09/111, arXiv:0907.4076. [Erratum: JHEP02,011(2010)].

[21] J. M. Campbell, R. K. Ellis, P. Nason, and E. Re, "Top-pair production and decay at NLO matched with parton showers", *JHEP* **04** (2015) 114, doi:10.1007/JHEP04(2015)114, arXiv:1412.1828.

[22] M. Czakon and A. Mitov, "Top++: A Program for the Calculation of the Top-Pair Cross-Section at Hadron Colliders", *Comput. Phys. Commun.* **185** (2014) 2930, doi:10.1016/j.cpc.2014.06.021, arXiv:1112.5675.

[23] T. Sjostrand, S. Mrenna, and P. Z. Skands, "A Brief Introduction to PYTHIA 8.1", *Comput. Phys. Commun.* **178** (2008) 852–867, doi:10.1016/j.cpc.2008.01.036, arXiv:0710.3820.

[24] CMS Collaboration, "Particle–flow event reconstruction in CMS and performance for jets, taus, and $E_{\mathrm{T}}^{\mathrm{miss}}$", CMS Physics Analysis Summary CMS-PAS-PFT-09-001, 2009.

[25] CMS Collaboration, "Commissioning of the particle-flow event reconstruction with the first LHC collisions recorded in the CMS detector", CMS Physics Analysis Summary CMS-PAS-PFT-10-001, 2010.

[26] K. Rose, "Deterministic annealing for clustering, compression, classification, regression and related optimisation problems", in *Proceedings of the IEEE*, volume 86, p. 86. 1998. doi:10.1109/5.726788.

[27] W. Waltenberger, R. Frühwirth, and P. Vanlaer, "Adaptive vertex fitting", *J. Phys. G* **34** (2007) N343, doi:10.1088/0954-3899/34/12/N01.

[28] CMS Collaboration, "Performance of electron reconstruction and selection with the CMS detector in proton-proton collisions at $\sqrt{s} = 8$ TeV", *JINST* **10** (2015), no. 06, P06005, doi:10.1088/1748-0221/10/06/P06005, arXiv:1502.02701.

[29] A. Hocker et al., "TMVA - Toolkit for Multivariate Data Analysis", *PoS* **ACAT** (2007) 040, arXiv:physics/0703039.

[30] CMS Collaboration, "Performance of CMS muon reconstruction in pp collision events at $\sqrt{s} = 7$ TeV", *JINST* **7** (2012) P10002, doi:10.1088/1748-0221/7/10/P10002, arXiv:1206.4071.

[31] M. Cacciari, G. P. Salam, and G. Soyez, "The anti-k_t jet clustering algorithm", *JHEP* **04** (2008) 063, doi:10.1088/1126-6708/2008/04/063, arXiv:0802.1189.

[32] M. Cacciari, G. P. Salam, and G. Soyez, "FastJet user manual", *Eur. Phys. J. C* **72** (2012) 1896, doi:10.1140/epjc/s10052-012-1896-2, arXiv:1111.6097.

[33] CMS Collaboration, "Algorithms for b Jet identification in CMS", CMS Physics Analysis Summary CMS-PAS-BTV-09-001, CERN, 2009. Geneva, Jul, 2009.

[34] CMS Collaboration, "Performance of tau-lepton reconstruction and identification in CMS", *JINST* **7** (2012) P01001, doi:10.1088/1748-0221/7/01/P01001, arXiv:1109.6034.

[35] CMS Collaboration, "Reconstruction and identification of τ lepton decays to hadrons and ν_τ at CMS", arXiv:1510.07488.

[36] L. Bianchini, J. Conway, E. K. Friis, and C. Veelken, "Reconstruction of the Higgs mass in H to tautau Events by Dynamical Likelihood techniques", *Journal of Physics: Conference Series* **513** (2014), no. 2, 022035.

[37] CMS Collaboration, "Measurement of the inclusive and differential tt production cross sections in lepton + jets final states at 13 TeV", CMS Physics Analysis Summary CMS-PAS-TOP-15-005, CERN, 2015.

[38] CMS Collaboration, "Performance of reconstruction and identification of tau leptons in their decays to hadrons and tau neutrino in LHC Run-2", CMS Physics Analysis Summary CMS-PAS-TAU-16-002, CERN, Geneva, 2016.